Multimodal image coregistration and inducible selective cell ablation to evaluate imaging ligands

John Virostko[a], Joseph Henske[b], Laurent Vinet[c], Smaragda Lamprianou[c], Chunhua Dai[b], Aramandla Radhika[b], Ronald M. Baldwin[a,d], Mohammad S. Ansari[d], Franz Hefti[e], Daniel Skovronsky[e], Hank F. Kung[f], Pedro L. Herrera[c], Todd E. Peterson[a,d], Paolo Meda[c], and Alvin C. Powers[b,g,h,1]

[a]Vanderbilt University Institute of Imaging Science, Vanderbilt University, Nashville, TN 37232; [b]Division of Diabetes, Endocrinology, and Metabolism, Department of Medicine, Vanderbilt University, Nashville, TN 37232; [c]Department of Cell Physiology and Metabolism, University of Geneva Medical School, 1211 Geneva 4, Switzerland; [d]Department of Radiology and Radiological Sciences, Vanderbilt University, Nashville, TN 37232; [e]Avid Radiopharmaceuticals, Inc., Philadelphia, PA 19104; [f]Departments of Radiology and Pharmacology, University of Pennsylvania, Philadelphia, PA 19104; [g]Department of Molecular Physiology and Biophysics, Vanderbilt University, Nashville, TN 37232; and [h]Veterans Affairs Tennessee Valley Healthcare System, Nashville, TN 37232

Edited by Michael E. Phelps, University of California, Los Angeles, CA, and approved November 2, 2011 (received for review June 15, 2011)

We combined multimodal imaging (bioluminescence, X-ray computed tomography, and PET), tomographic reconstruction of bioluminescent sources, and two unique, complementary models to evaluate three previously synthesized PET radiotracers thought to target pancreatic beta cells. The three radiotracers {[^{18}F]fluoropropyl-(+)-dihydrotetrabenazine ([^{18}F]FP-DTBZ), [^{18}F](+)-2-oxiranyl-3-isobutyl-9-(3-fluoropropoxy)-10-methoxy-2,3,4,6,7,11b-hexahydro-1H-pyrido[2,1-a]isoquinoline (^{18}F-AV-266), and (2*S*,3*R*,11b*R*)-9-(3-fluoropropoxy)-2-(hydroxymethyl)-3-isobutyl-10-methoxy-2,3,4,6,7,11b-hexahydro-1*H*-pyrido[2,1-*a*]isoquinolin-2-ol (^{18}F-AV-300)} bind vesicular monoamine transporter 2. Tomographic reconstruction of the bioluminescent signal in mice expressing luciferase only in pancreatic beta cells was used to delineate the pancreas and was coregistered with PET and X-ray computed tomography images. This strategy enabled unambiguous identification of the pancreas on PET images, permitting accurate quantification of the pancreatic PET signal. We show here that, after conditional, specific, and rapid mouse beta-cell ablation, beta-cell loss was detected by bioluminescence imaging but not by PET imaging, given that the pancreatic signal provided by three PET radiotracers was not altered. To determine whether these ligands bound human beta cells in vivo, we imaged mice transplanted with luciferase-expressing human islets. The human islets were imaged by bioluminescence but not with the PET ligands, indicating that these vesicular monoamine transporter 2-directed ligands did not specifically bind beta cells. These data demonstrate the utility of coregistered multimodal imaging as a platform for evaluation and validation of candidate ligands for imaging islets.

diabetes | insulin | molecular imaging | pancreatic islet | bioluminescence tomography

The ability to image and quantify rare cell populations would aid diagnosis and treatment of Parkinson disease (1), Alzheimer's disease (2), certain cancers (3), and diabetes mellitus (4). In the case of diabetes, the rare cell population of interest is the pancreatic beta cell, the sole cell type capable of synthesizing and releasing the hormone insulin in vertebrates. Reduced beta-cell mass is a cardinal feature of type 1 diabetes (5) and is now recognized as a critical feature in type 2 diabetes as well (6–8), but we cannot noninvasively quantify beta-cell mass in humans. Despite the efforts of a number of investigators, approaches for noninvasive assessment of beta-cell mass in vivo are presently limited. The small size of pancreatic islets (50–300 μm in diameter), their sparse frequency (1–2% of pancreatic mass), and their scattered distribution throughout the pancreas create a number of scientific and technical challenges for noninvasive imaging and quantification of beta-cell mass. Additionally, the location of the pancreas deep within the abdomen, its proximity to other major organs, and artifacts from respiratory, cardiac, and intestinal motion pose further challenges to imaging beta cells.

The dynamic changes in beta-cell mass accompanying diabetes are neither well understood nor well characterized by functional measurements of glycemic control. Although the amount of insulin/C-peptide secreted after a glucose or meal challenge gives insight into insulin secretory capacity (4, 9), these only indirectly reflect beta-cell mass and do not determine whether this mass is increasing or declining. For example, glucose homeostasis is unaffected until beta-cell mass is reduced to less than half its original value, presumably because of a large functional reserve capacity, and overt diabetes develops only when beta-cell mass is greatly reduced (10–12). Morphometric analysis of histological sections (13) requires removal of the pancreas to quantify beta-cell mass. Because we incompletely understand the time course and development of both forms of diabetes, our ability is limited to effectively test interventions to prevent beta-cell loss. Furthermore, efforts to regenerate beta-cell mass (14, 15) would be aided by the ability to image the beta cells both during preclinical development of regenerative protocols and during clinical monitoring of therapeutic response.

Recently, the vesicular monoamine transporter 2 (VMAT2) has been identified as a possible target for noninvasive positron-emission tomography (PET) imaging of pancreatic beta cells. Gene-expression studies on human tissues indicate that VMAT2 expression is greater in islets than in the exocrine tissue of the pancreas (16), and immunohistochemical studies have shown costaining of VMAT2 and insulin (17, 18). A radiolabeled ligand to VMAT2, dihydrotetrabenazine ([^{11}C]DTBZ) (19), has been extensively used in PET imaging of both human and rodent brains, revealing altered density of VMAT2 in diseased states such as Parkinson disease (20). [^{11}C]DTBZ has also been used for pancreatic islet imaging, showing reduced pancreatic uptake in rodent models of autoimmune and streptozotocin-induced diabetes (21, 22). Imaging in humans has demonstrated lower pancreatic [^{11}C]DTBZ radioactivity in type 1 diabetics (23). However, [^{11}C]DTBZ has high nonspecific binding to the exocrine pancreas, suggesting that it may not be suitable for imaging beta-cell mass (24, 25). An ^{18}F-labeled analog of DTBZ ([^{18}F]DTBZ) has been previously synthesized (26), and the longer half-life of ^{18}F (110 min versus 20 min for ^{11}C) facilitates imaging at longer intervals after radiotracer administration, allowing more

Author contributions: J.V., J.H., R.M.B., M.S.A., F.H., D.S., H.F.K., T.E.P., P.M., and A.C.P. designed research; J.V., J.H., L.V., S.L., C.D., A.R., and R.M.B. performed research; H.F.K. and P.L.H. contributed new reagents/analytic tools; J.V., P.M., and A.C.P. analyzed data; and J.V., T.E.P., P.M., and A.C.P. wrote the paper.

Conflict of interest statement: F.H., D.S., and H.F.K. either are employed at Avid Radiopharmaceuticals or have a financial interest in the company. A.C.P. has received an investigator-initiated research grant from Eli Lilly and Company.

This article is a PNAS Direct Submission.

Freely available online through the PNAS open access option.

[1]To whom correspondence should be addressed. E-mail: al.powers@vanderbilt.edu.

This article contains supporting information online at www.pnas.org/lookup/suppl/doi:10.1073/pnas.1109480108/-/DCSupplemental.

time for clearance of unbound radiotracer, thereby possibly exhibiting lower nonspecific pancreatic binding.

Molecular imaging, an emerging discipline involving the visualization and measurement of biological processes, has great potential for imaging the pancreatic beta cell. Because each molecular imaging modality has inherent strengths and limitations, a multimodal approach encompassing several imaging modalities can provide complementary quantitative and spatial information. We reasoned that the evaluation of molecular imaging agents targeting beta cells would benefit from both multimodal molecular imaging and controllable manipulation of the cell population. Toward this end, we created mice with beta-cell–specific expression of luciferase (27) and the human diphtheria toxin receptor (DTR) (28) that we termed MIP-Luc-VU/RIP-DTR mice (*Methods*). In this model, the bioluminescence, which emanates solely from the beta cells in the pancreas and can be noninvasively imaged with bioluminescence imaging (BLI), correlates with beta-cell mass (27). Administration of diphtheria toxin (DT) induces rapid, complete, and specific beta-cell ablation (28). In this article, we highlight the utility of this mouse model and an immunodeficient mouse model transplanted with luciferase-transduced human islets for evaluation of three [^{18}F]DTBZ analogs with differing pharmacokinetics, and we demonstrate the utility of the multimodal imaging strategy for screening of candidate imaging probes.

Results

Bioluminescence Tomography and Coregistration with PET/X-Ray Computed Tomography (CT) Enable Unambiguous Delineation of Rodent Pancreas. We placed MIP-Luc-VU/RIP-DTR mice between transparent acrylic plates to facilitate imaging from the ventral and dorsal sides of the mouse and performed BLI at six different wavelengths on each side (Fig. S1*A*). We then transported the mouse, still immobilized between acrylic plates, to scanners for PET and CT imaging. We then created 2D projection images of the ventral and dorsal sides of the mouse from the 3D CT image. We next mapped the 2D bioluminescent images of the ventral and dorsal sides of the MIP-Luc-VU/RIP-DTR mouse to the 2D CT projection images (Fig. S1*A*), which allowed us to determine the bioluminescence intensity at each point on the surface of the CT image (Fig. S1*B*) at six different wavelengths. We then used an algorithm to locate the bioluminescence source location in 3D space (29) to reconstruct the bioluminescent signal within the CT image space (Fig. S1*B*).

PET/CT imaging of MIP-Luc-VU/RIP-DTR mice after administration of [^{18}F]fluoropropyl-(+)-dihydrotetrabenazine ([^{18}F]FP-DTBZ; termed ^{18}F-AV-133) showed uptake not only in the pancreas but also in the liver, intestines, spleen, and bladder (Fig. 1*B*) as well as in a few regions of the central nervous system, presumably the basal ganglia target areas of dopaminergic neurons, including corpus striatum and nucleus accumbens (Fig. S2). The proximity of the abdominal set of organs to the pancreas prevented the accurate delineation of a region of interest (ROI) encompassing solely the pancreas on PET images. To address this problem, we performed bioluminescence tomography of MIP-Luc-VU/RIP-DTR mice (Fig. 1*A*) and coregistered this reconstruction (Fig. 1*C*), which demonstrated bioluminescence only in the pancreas (Fig. 1*D*), with PET and CT images of the same axial slices (Fig. 1*E*). The PET/CT coregistration of the axial slice showed [^{18}F]FP-DTBZ uptake in the pancreas and in neighboring organs (Fig. 1*E*). An ROI comprising only the pancreas (red dashed line in Fig. 1 *D* and *E*) was defined by using the tomographic bioluminescence image (Fig. 1*D*) and coregistered with the corresponding [^{18}F]FP-DTBZ PET image (Fig. 1*E*). This coregistration allowed for unambiguous delineation of the pancreas ROI in the [^{18}F]FP-DTBZ PET image (Fig. 1 *D* and *E*), which enabled us to quantify the pancreatic PET signal while minimizing the confounding influence of the [^{18}F]FP-DTBZ signal from adjacent organs.

DT Results in Beta-Cell Ablation, Which Is Detected by BLI but Not by [^{18}F]FP-DTBZ PET Imaging. After DT administration, MIP-Luc-VU/RIP-DTR mice had near complete beta-cell destruction (Fig. 2*A*) and developed severe hyperglycemia (Fig. 2*B* and Fig. S3). Consistently, these DT-treated mice displayed a marked decrease in pancreatic bioluminescence intensity (Fig. 2 *C* and *D*). In contrast, PET imaging of the same mice with [^{18}F]FP-DTBZ revealed that the pancreatic signal did not change (Fig. 2*E*). Likewise, the biodistribution of [^{18}F]FP-DTBZ, as assessed by well-counter measurements of radioactivity in dissected organs, was not affected by DT treatment (Fig. 2*F*). Postmortem measurement confirmed that the pancreatic insulin of DT-treated

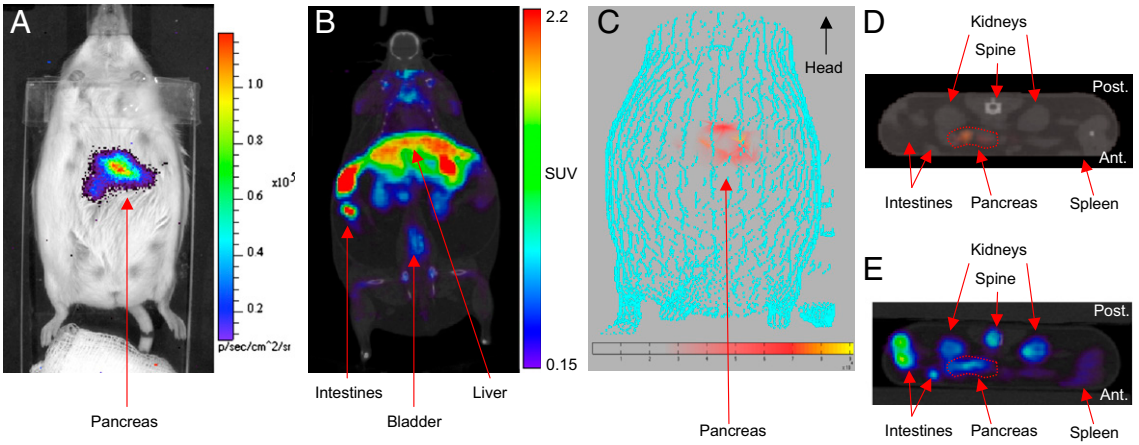

Fig. 1. Coregistration of bioluminescence tomography and PET images permits evaluation of pancreatic [^{18}F]FP-DTBZ uptake. (*A*) After luciferin injection, bioluminescence emanates from the pancreas of a MIP-Luc-VU/RIP-DTR mouse. (*B*) [^{18}F]FP-DTBZ PET/CT image of the same mouse displays [^{18}F]FP-DTBZ accumulation in several abdomen organs, including the liver, bladder, and intestines. (*C*) Reconstructed bioluminescence tomography of the same mouse displays the bioluminescence source location (red) within the CT mouse volume (blue pixels). (*D*) An axial slice through the tomographic bioluminescence image reveals the reconstructed bioluminescence source location in the expected anatomical location of the pancreas. The dashed red line defines the pancreatic ROI based on the bioluminescence reconstruction. (*E*) PET/CT of the same slice displays [^{18}F]FP-DTBZ uptake in the kidneys, intestines, spleen, spine, and pancreas. The pancreatic ROI (dashed red line) from *D* is overlaid on the PET/CT image, demonstrating the pancreatic coregistration of bioluminescence and [^{18}F]FP-DTBZ PET signal of the pancreas.

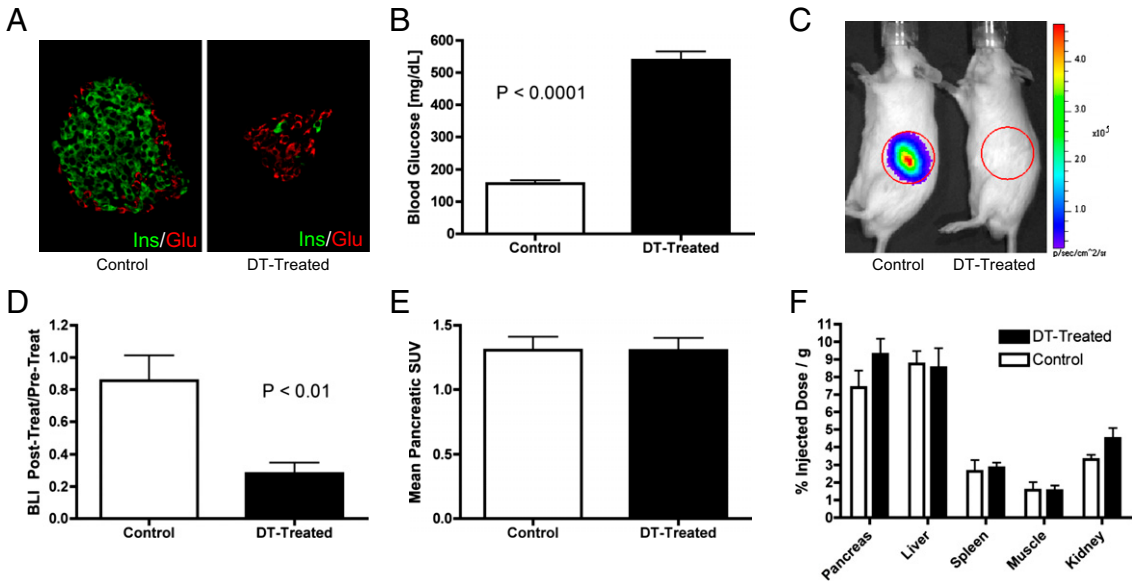

Fig. 2. DT treatment ablates beta cells and bioluminescence signal but not pancreatic [^{18}F]FP-DTBZ PET accumulation. (*A*) An islet from a control, untreated mouse (*Left*) displays normal insulin-expressing beta (green) and glucagon-expressing alpha (red) cells. After DT administration (*Right*), an islet displays almost complete loss of beta (green) and the persistence of alpha (red) cells. (*B*) MIP-Luc-VU/RIP-DTR mice treated with DT exhibited significantly increased ($P <$ 0.0001) blood glucose at 4 d after DT administration (black bar) compared with normoglycemic untreated, control mice (white bar). (*C*) BLI of a control untreated mouse (*Left*) reveals photon emission from the pancreas. This signal was abolished at 4 d after DT treatment (*Right*). (*D*) Quantitative analysis showed a significant reduction ($P < 0.01$) of BLI after this treatment. (*E*) In contrast, the pancreatic uptake of [^{18}F]FP-DTBZ, as evaluated from the PET signal, was similar in control and DT-treated mice. (*F*) Ex vivo biodistribution of [^{18}F]FP-DTBZ was similar in organs dissected from DT-treated (black bars) and untreated MIP-Luc-VU/RIP-DTR mice (white bars). *B* and *D–F* display the mean + SE data of six mice per group.

mice was significantly reduced compared with that of untreated control mice (Fig. S4*A*). Consistent with the PET and BLI results, DT treatment of MIP-Luc-VU/RIP-DTR mice decreased the mRNA levels for insulin I and insulin II, but not VMAT2, in total pancreatic RNA (Fig. S4*B*). These results strongly suggested that [^{18}F]FP-DTBZ was binding to the mouse pancreas but not to pancreatic beta cells.

Two unique VMAT2-targeted ligands were synthesized with chemical modifications intended to increase affinity to VMAT2 and to improve in vivo pharmacokinetics compared with [^{18}F]FP-DTBZ. Chemical structures of these two ligands, dubbed [^{18}F](+)-2-oxiranyl-3-isobutyl-9-(3-fluoropropoxy)-10-methoxy-2,3,4,6,7,11b-hexahydro-1H-pyrido[2,1-a]isoquinoline (^{18}F-AV-266) and (2*S*,3*R*,11b*R*)-9-(3-fluoropropoxy)-2-(hydroxymethyl)-3-isobutyl-10-methoxy-2,3,4,6,7,11b-hexahydro-1*H*-pyrido[2,1-*a*]isoquinolin-2-ol (^{18}F-AV-300), are shown in Fig. S5. ^{18}F-AV-266 and ^{18}F-AV-300 were tested exactly as described above. As found with [^{18}F]FP-DTBZ, despite DT inducing beta-cell destruction and loss of bioluminescence, neither the pancreatic PET signal nor the biodistribution of ^{18}F-AV-266 and ^{18}F-AV-300 were altered by beta-cell loss (Figs. S6 and S7, respectively). Altogether, the results with the MIP-Luc-VU/RIP-DTR model indicate that three VMAT2-directed ligands bind to the mouse pancreas greater than to several other tissues, except liver, but that the pancreatic signal is not caused by binding to beta cells.

Transplanted Human Islets Are Imaged by BLI but Not by [^{18}F]FP-DTBZ PET. To determine whether human islets could be imaged by [^{18}F]FP-DTBZ PET, we transplanted luciferase-expressing human islets (30) beneath the left kidney capsule of immunodeficient mice. We have previously shown that BLI in this model is present for months and correlates with transplanted islet number (30). As expected, BLI was specific, with no bioluminescence detected from the right kidney, which received no islet graft, or other organs (Fig. 3*A*). [^{18}F]FP-DTBZ PET imaging of the same transplanted mice displayed radiotracer clearance in the renal pelvis of both the islet graft-bearing kidney and the contralateral kidney, indicating comparable blood flow (Fig. 3*B*). However, no PET signal was detected at the distal pole of the left kidney where the islet graft was implanted (Fig. 3*B*) and later observed after a nephrectomy at the end of the imaging session (Fig. 3*C*). No significant difference in the renal PET signal from the islet graft-bearing kidney and the contralateral kidney was observed (Fig. 3*D*). Similarly, postmortem biodistribution of the radiotracer showed no difference between the graft-bearing kidney and the contralateral kidney (Fig. 3*E*). Furthermore, after excision from the surrounding renal tissue, the islet graft did not display a quantifiable retention of the radiotracer, as assessed by well-counter measurements. Similar results were obtained with both the ^{18}F-AV-266 and ^{18}F-AV-300 probes (Fig. S8). Isolated mouse and human islets and the retrieved human islet transplant grafts expressed VMAT2 mRNA, but VMAT2 expression was much lower in mouse pancreatic islets compared with human islets or the mouse adrenal gland, which is known to express high levels of VMAT2 (Fig. S9 *A* and *B*).

Discussion

We developed two complementary models that combine multimodal imaging, mouse and human islets, tomographic reconstruction of bioluminescent images, and targeted cell ablation for evaluating imaging probes targeting the pancreatic beta cells. Because the noninvasive delineation of the pancreas is difficult in the living mouse, the tomographic reconstruction of bioluminescent beta cells in MIP-Luc-VU/RIP-DTR mice and the coregistration of bioluminescence tomography with PET and CT show that a bioluminescent signal can be used as an anatomic reference for identifying small cell populations and intermixed organs in other coregistered imaging modalities. This strategy enabled accurate delineation of a pancreatic ROI on PET images, which is particularly useful when evaluating signals from the abdomen, for which CT contrast of soft tissue is low and neighboring organs may accumulate or clear the imaging agent.

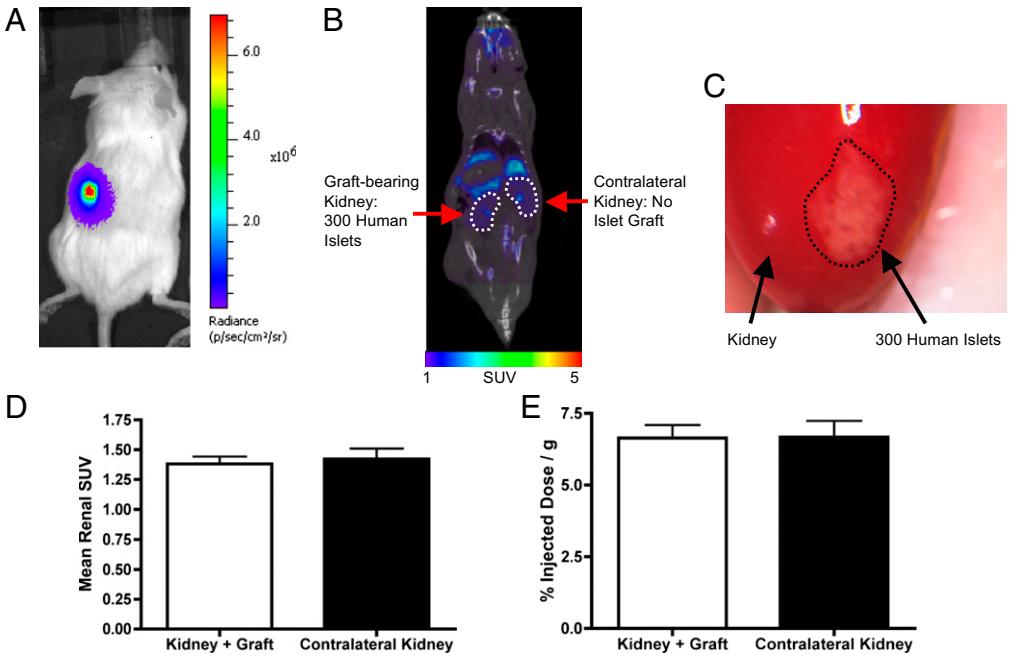

Fig. 3. Human islets are detected by BLI but not by [^{18}F]FP-DTBZ PET imaging. (*A*) Mice with human islets transduced with luciferase and transplanted beneath the left renal capsule emit bioluminescence. (*B*) Coronal PET/CT slice of a mouse bearing transplanted human islets in the left renal capsule after [^{18}F]FP-DTBZ administration. No difference is detectable between the left kidney, which was grafted with 300 islets, and the right kidney, which was not grafted. Both kidneys are delineated by a white dashed line. (*C*) Postmortem image of the left kidney reveals the persistence of the human islet graft (whitish area outlined with a black dashed line) underneath the kidney capsule at the end of the multimodal BLI/CT/PET imaging. (*D*) The renal uptake of [^{18}F]FP-DTBZ, as evaluated from the PET signal, was similar in the left kidney containing transplanted human islets and the contralateral control right kidney. (*E*) Ex vivo biodistribution of [^{18}F]FP-DTBZ was similar in the islet graft containing left kidney and the control right kidney. *D* and *E* display the mean + SE data of six mice per group.

By combining beta-cell–specific BLI and diphtheria receptor expression, we were able to manipulate beta-cell mass by rapid, selective, and complete beta-cell destruction (28) and noninvasively assay this alteration with BLI. Additionally, this approach avoids the pleiotropic effects of streptozotocin, a drug widely used to induce beta-cell destruction that is also toxic to several organs (31, 32) and may affect radiotracer biodistribution and clearance. We used these alternative approaches and models to evaluate a family of PET radiotracers that bind VMAT2, a target predicted to be useful for noninvasive imaging of the pancreatic beta cell.

Previous studies investigating radiolabeled DTBZ analogs for imaging the beta cell have led to contradictory conclusions. Studies in rodent models (21, 22, 25) and humans (23) have demonstrated a decrease in radiotracer retention in the pancreas of diabetics. However, other groups have found high radiotracer binding to the exocrine pancreas of rodents and humans (24, 33, 34) with reduced exocrine binding in the diabetic pancreas (24). Using multimodal imaging and inducible and selective beta-cell ablation, we demonstrate that the PET signal from radiolabeled VMAT2 ligands in the mouse pancreas does not correlate with beta-cell mass. Despite the loss of beta cells after DT administration, as monitored by BLI, mice with reduced beta-cell mass did not exhibit lower pancreatic retention of three different [^{18}F]DTBZ analogs. The different [^{18}F]DTBZ analogs were chemically modified to alter their in vivo pharmacokinetics and to improve their pancreatic biodistribution and binding. Despite all three probes being concentrated in the pancreas compared with other tissues, this binding was not the result of beta-cell binding. A possible explanation for the pancreatic accumulation of the VMAT2 probes is binding to pancreatic cells other than beta cells, which is consistent with the expression of VMAT2 in several nonendocrine cell types, such as neurons (18), and with the high nondisplaceable binding of [^{18}F]fluoroethyl-dihydrotetrabenazine, a close analog of [^{18}F]FP-DTBZ, to human pancreatic exocrine tissue in vitro (33). This latter finding, when combined with the observation that streptozotocin also reduces the binding of [^{11}C]DTBZ to pancreatic exocrine tissue (24), may account for the reduced binding of [^{11}C]DTBZ after streptozotocin that was noted in previous reports (21, 25).

In a preclinical model, we found that transplanted human islets were readily detectable in living mice by BLI, but not by imaging with either [^{18}F]FP-DTBZ PET or two other DTBZ analogs. A caveat to these results is that the human islets in this transplantation model might have different features from islets in the pancreas, e.g., a different expression of VMAT2 or were fewer in number than islets of the human pancreas. However, we detected VMAT2 mRNA in the human islet grafts. Although there is variability in human islet preparations, the humans islets we transplanted were from three different preparations, each of which had glucose-stimulated insulin secretion, as assessed by islet perifusion. Another caveat is the access of the imaging probe, which might be limited in transplanted islets. However, because both oxygen and the injected substrate luciferin are necessary for BLI (35), the bioluminescence of the human islet grafts indicates that the transplanted islets were viable and revascularized after transplantation. In addition, because target density affects PET imaging, a further caveat may be that the transplanted islets might not have a sufficient density. However, transplanted islets engraft in a contiguous area beneath the renal capsule, reaching a target density exceeding that of native human islets in the pancreas.

Altogether, the data from our complementary imaging models suggest that three DTBZ ligands may not be suitable for noninvasive imaging of islets in humans because of nonspecific, off-target binding. VMAT2 may still be a suitable target for beta-cell imaging, but new probes or ligands targeting VMAT2 are needed. Species-specific differences in the expression levels of VMAT2 may also contribute to the different imaging observations with

DTBZ ligands, particularly when human and rodent data are compared. Human islets express higher levels of VMAT2 than murine islets do, emphasizing a potential limitation of rodent models to assess islet-imaging ligands as well as the utility of our complementary models using both mouse and human islets.

The experimental strategy we describe here should facilitate the in vivo screening of imaging agents targeting pancreatic beta cells because it combines an extremely sensitive imaging modality in BLI with DT-mediated targeted cell ablation and human islet imaging. The development of imaging ligands is a lengthy process that usually involves identification of a target molecule, in vitro testing, and validation in preclinical models before human studies. Unfortunately, cell and in vitro studies may not predict in vivo imaging results (36). For example, autoradiography with DTBZ analogs in the pancreas has yielded conflicting results (24, 33, 34). Despite the significantly higher resolution of autoradiography compared with PET imaging, autoradiography is not able to distinguish individual beta cells, and its quantitation does not necessarily predict PET imaging results. Furthermore, human and mouse cells may express different levels of a target molecule or a different affinity for a ligand. Importantly, our model system, integrating both mouse beta cells and human islets in vivo as well as multimodal imaging, overcomes some of these experimental limitations and should allow preclinical testing of new islet-targeted ligands. Although this experimental approach was developed for testing agents thought to target pancreatic beta cells, the expression of the DTR and luciferase genes under control of other cell-specific promoters should also be useful in developing other new models for the in vivo imaging of other sparse cell types.

Methods

Mouse Models. We bred mice expressing the luciferase optical reporter cDNA Luc under control of the 9.2-kb mouse insulin I promoter (MIP) (27) with mice expressing the human DTR, human heparin-binding EGF-like growth factor, under control of the rat insulin promoter (RIP) (28) to produce double-transgenic mice termed MIP-Luc-VU/RIP-DTR. MIP-Luc-VU/RIP-DTR mice were on an FVB background (Nashville colony), except for those used in the studies shown in Fig. S3C, which were on a C57BL6 background (Geneva colony). Studies were performed on the Nashville colony unless otherwise noted. In most experiments, male mice were rendered diabetic by a single i.p. injection of 125 ng of DT (List Biological Laboratories) as previously described (28). Reconstituted toxin was diluted in 2.5 ng/μL sterile water and injected as a volume of 50 μL. In the experiments shown in Fig. S3C, male and female mice received three injections of the same DT dose at 2-d intervals. Throughout the experiment, nonfasting blood glucose measurements were obtained from tail-vein blood measured with an Accu-Chek glucose meter (Roche Diagnostics).

Human Islet Transplantation Model. Human islets, obtained from the Islet Cell Resource Centers of the Integrated Islet Distribution Program (http://iidp.coh.org) were delivered by overnight courier to Vanderbilt University and assessed for viability in a cell-perifusion system (37). Human islet function was verified by ensuring that insulin secretion increased more than fourfold in response to an increase in glucose from 2.8 to 16.8 mM or 16.8 mM glucose plus 0.045 mM isobutylmethylxanthine. Islets were transduced overnight with an adenovirus (Adv-luciferase) that bicistronically encodes firefly luciferase (luc) and GFP under the control of the CMV promoter, as previously described (30). Nondiabetic, immunodeficient mice [NOD-scid IL2rg-null (NSG); The Jackson Laboratory] were used as transplant recipients (30, 38). Three hundred human islets were injected beneath the capsule of the left kidney as previously described (30, 37). PET imaging was performed on mice bearing human islets at ~6 wk after this transplantation.

BLI. Mice were injected once i.p. with 150 mg/kg D-luciferin (at a concentration of 15 mg/mL) (27). Mice were anesthetized with 1.5% isoflurane and placed in the imaging chamber of an IVIS 200 CCD camera (Caliper). Bioluminescence images were captured with 1 min integration time for 10 min after the luciferin injection. Peak bioluminescence emission was quantified by summing bioluminescence intensity within an ROI centered over the pancreas as previously described (27).

Synthesis of VMAT2-Directed Ligands. The DTBZ analog [^{18}F]FP-DTBZ (^{18}F-AV-133) was prepared with fluorine-18 using precursors supplied by Avid Radiopharmaceuticals (39). Detailed radiochemical synthesis is provided in *SI Methods*. ^{18}F-AV-266 and ^{18}F-AV-300 were similarly prepared, and their chemical structures are shown in Fig. S5.

PET/CT Imaging. The radiotracers were administered via a single retroorbital injection of ~1 mCi (~200 μL). Retroorbital injection of the radiotracer results in similar biodistribution as i.v. tail-vein injection, with an easier procedure and reduced soft-tissue extravasation (40). After a 40-min distribution period, mice were anesthetized with 1.5% isoflurane and placed in a microPET Focus 220 scanner (Siemens) for a 20-min static PET scan. A CT image of each mouse was created with a microCT scanner (Imtek). PET images were reconstructed using a 2D filtered back-projection algorithm. Three-dimensional ROIs were drawn around the pancreas with AMIDE software (41).

Multimodal Imaging and Bioluminescence Tomography. Anesthetized mice were immobilized between two transparent acrylic plates, which enabled image acquisition from both the ventral and dorsal sides of the animals. Dorsal and ventral spectrally filtered images were taken through six 20-nm bandpass filters at wavelengths from 560 to 660 nm by using the IVIS 200 CCD camera. The mouse was then transferred to the microPET and microCT scanners, in which images were taken as outlined above, and coregistered with markers embedded within the animal holder. A dorsal and ventral projection CT image was generated and coregistered with the dorsal and ventral optical images by using a mutual information algorithm (42). The 2D optical data were then mapped to the surface points of the CT image, using these projection images to create a 3D distribution of optical data on the surface of the mouse (Fig. S1). A triangular finite element mesh was generated from the CT image with MatLab software (Mathworks). The internal bioluminescence source distribution was then reconstructed from the surface light map with MatLab by solving the NIRFAST inverse diffusion approximation of light propagation (29).

Ex Vivo Biodistribution of Radiotracer. Immediately after imaging, the mice were euthanized, and the pancreas, liver, spleen, kidneys, and quadriceps femoris were excised, weighed, and counted in a calibrated scintillation well counter (Capintec). Regional uptake was calculated as percentage injected dose per gram by dividing the decay-corrected radioactivity in each tissue by its weight and by the injected dose.

Statistical Analysis. An unpaired, two-tailed *t* test was used to compare the experimental results. Data are expressed as means ± SE.

Quantitative RT-PCR. Quantitative RT-PCR was performed as described in *SI Methods*, and TaqMan primers/probes for real-time PCR are given in Table S1.

ACKNOWLEDGMENTS. Human islets were obtained from the Integrated Islet Distribution Program (http://iidp.coh.org), which is supported by the National Institute of Diabetes and Digestive and Kidney Diseases and the Juvenile Diabetes Research Foundation. This study was supported by Juvenile Diabetes Research Foundation Grants 1-2003-170, 37-2009-59, 1-2006-874, 26-2008-892, and 40-2011-11; Swiss National Science Foundation Grants 310000-109402, 310000-122423, and 1Z73ZO-127935CR32I3129987; European Union Grants BETAIMAGE 222980 and Innovative Medicines Initiative for Diabetes (IMIDIA), C2008-T7; grants from the Veterans Affairs Research Service; National Institutes of Health Grants DK072473, DK66636, DK68764, DK68854, DK69603, DK089572, and T32EB001628; South-Eastern Center for Small-Animal Imaging Grant U24CA126588; Vanderbilt Mouse Metabolic Phenotyping Center Grant DK59637; and Vanderbilt Diabetes Research and Training Center Grant DK20593.

1. Calne DB, et al. (1985) Positron emission tomography after MPTP: Observations relating to the cause of Parkinson's disease. *Nature* 317:246–248.
2. Backskai BJ, et al. (2003) Four-dimensional multiphoton imaging of brain entry, amyloid binding, and clearance of an amyloid-β ligand in transgenic mice. *Proc Natl Acad Sci USA* 100:12462–12467.
3. Som P, et al. (1980) A fluorinated glucose analog, 2-fluoro-2-deoxy-D-glucose (F-18): Nontoxic tracer for rapid tumor detection. *J Nucl Med* 21:670–675.
4. Robertson RP (2007) Estimation of β-cell mass by metabolic tests: Necessary, but how sufficient? *Diabetes* 56:2420–2424.
5. Gepts W (1965) Pathologic anatomy of the pancreas in juvenile diabetes mellitus. *Diabetes* 14:619–633.

6. Butler AE, et al. (2003) β-Cell deficit and increased β-cell apoptosis in humans with type 2 diabetes. *Diabetes* 52:102–110.
7. Hanley SC, et al. (2010) β-Cell mass dynamics and islet cell plasticity in human type 2 diabetes. *Endocrinology* 151:1462–1472.
8. Rahier J, Guiot Y, Goebbels RM, Sempoux C, Henquin JC (2008) Pancreatic β-cell mass in European subjects with type 2 diabetes. *Diabetes Obes Metab* 10(Suppl 4):32–42.
9. McCulloch DK, Koerker DJ, Kahn SE, Bonner-Weir S, Palmer JP (1991) Correlations of in vivo beta-cell function tests with beta-cell mass and pancreatic insulin content in streptozocin-administered baboons. *Diabetes* 40:673–679.
10. Bonner-Weir S, Trent DF, Weir GC (1983) Partial pancreatectomy in the rat and subsequent defect in glucose-induced insulin release. *J Clin Invest* 71:1544–1553.
11. Larsen MO, Rolin B, Wilken M, Carr RD, Gotfredsen CF (2003) Measurements of insulin secretory capacity and glucose tolerance to predict pancreatic β-cell mass in vivo in the nicotinamide/streptozotocin Göttingen minipig, a model of moderate insulin deficiency and diabetes. *Diabetes* 52:118–123.
12. Saito K, Yaginuma N, Takahashi T (1979) Differential volumetry of A, B and D cells in the pancreatic islets of diabetic and nondiabetic subjects. *Tohoku J Exp Med* 129:273–283.
13. Davalli AM, et al. (1995) Early changes in syngeneic islet grafts: Effect of recipient's metabolic control on graft outcome. *Transplant Proc* 27:3238–3239.
14. Nir T, Melton DA, Dor Y (2007) Recovery from diabetes in mice by β cell regeneration. *J Clin Invest* 117:2553–2561.
15. Xu G, Stoffers DA, Habener JF, Bonner-Weir S (1999) Exendin-4 stimulates both beta-cell replication and neogenesis, resulting in increased β-cell mass and improved glucose tolerance in diabetic rats. *Diabetes* 48:2270–2276.
16. Maffei A, et al. (2004) Identification of tissue-restricted transcripts in human islets. *Endocrinology* 145:4513–4521.
17. Anlauf M, et al. (2003) Expression of the two isoforms of the vesicular monoamine transporter (VMAT1 and VMAT2) in the endocrine pancreas and pancreatic endocrine tumors. *J Histochem Cytochem* 51:1027–1040.
18. Weihe E, Eiden LE (2000) Chemical neuroanatomy of the vesicular amine transporters. *FASEB J* 14:2435–2449.
19. DaSilva JN, Kilbourn MR (1992) In vivo binding of [^{11}C]tetrabenazine to vesicular monoamine transporters in mouse brain. *Life Sci* 51:593–600.
20. Frey KA, Koeppe RA, Kilbourn MR (2001) Imaging the vesicular monoamine transporter. *Adv Neurol* 86:237–247.
21. Simpson NR, et al. (2006) Visualizing pancreatic β-cell mass with [^{11}C]DTBZ. *Nucl Med Biol* 33:855–864.
22. Souza F, et al. (2006) Longitudinal noninvasive PET-based β cell mass estimates in a spontaneous diabetes rat model. *J Clin Invest* 116:1506–1513.
23. Goland R, et al. (2009) ^{11}C-dihydrotetrabenazine PET of the pancreas in subjects with long-standing type 1 diabetes and in healthy controls. *J Nucl Med* 50:382–389.
24. Fagerholm V, et al. (2010) Assessment of islet specificity of dihydrotetrabenazine radiotracer binding in rat pancreas and human pancreas. *J Nucl Med* 51:1439–1446.
25. Singhal T, et al. (2011) Pancreatic beta cell mass PET imaging and quantification with [^{11}C]DTBZ and [^{18}F]FP-(+)-DTBZ in rodent models of diabetes. *Mol Imaging Biol* 13: 973–984.
26. Kung MP, et al. (2007) Characterization of optically resolved 9-fluoropropyl-dihydrotetrabenazine as a potential PET imaging agent targeting vesicular monoamine transporters. *Nucl Med Biol* 34:239–246.
27. Virostko J, et al. (2010) Bioluminescence imaging in mouse models quantifies β cell mass in the pancreas and after islet transplantation. *Mol Imaging Biol* 12:42–53.
28. Thorel F, et al. (2010) Conversion of adult pancreatic α-cells to β-cells after extreme β-cell loss. *Nature* 464:1149–1154.
29. Dehghani H, Davis SC, Pogue BW (2008) Spectrally resolved bioluminescence tomography using the reciprocity approach. *Med Phys* 35:4863–4871.
30. Fowler M, et al. (2005) Assessment of pancreatic islet mass after islet transplantation using in vivo bioluminescence imaging. *Transplantation* 79:768–776.
31. Kume E, et al. (2004) Hepatic changes in the acute phase of streptozotocin (SZ)-induced diabetes in mice. *Exp Toxicol Pathol* 55:467–480.
32. Sadoff L (1970) Nephrotoxicity of streptozotocin (NSC-85998). *Cancer Chemother Rep* 54:457–459.
33. Eriksson O, et al. (2010) In vivo and in vitro characterization of [^{18}F]-FE-(+)-DTBZ as a tracer for beta-cell mass. *Nucl Med Biol* 37:357–363.
34. Tsao HH, et al. (2010) Binding characteristics of 9-fluoropropyl-(+)-dihydrotetrabenzazine (AV-133) to the vesicular monoamine transporter type 2 in rats. *Nucl Med Biol* 37:413–419.
35. Contag PR, Olomu IN, Stevenson DK, Contag CH (1998) Bioluminescent indicators in living mammals. *Nat Med* 4:245–247.
36. Sweet IR, et al. (2004) Systematic screening of potential β-cell imaging agents. *Biochem Biophys Res Commun* 314:976–983.
37. Brissova M, et al. (2004) Intraislet endothelial cells contribute to revascularization of transplanted pancreatic islets. *Diabetes* 53:1318–1325.
38. Brehm MA, et al. (2010) Human immune system development and rejection of human islet allografts in spontaneously diabetic NOD-*Rag1^{null} IL2rγ^{null} Ins2^{Akita}* mice. *Diabetes* 59:2265–2270.
39. Kung MP, et al. (2008) In vivo imaging of β-cell mass in rats using ^{18}F-FP-(+)-DTBZ: A potential PET ligand for studying diabetes mellitus. *J Nucl Med* 49:1171–1176.
40. Nanni C, et al. (2007) Retro-orbital injection is an effective route for radiopharmaceutical administration in mice during small-animal PET studies. *Nucl Med Commun* 28:547–553.
41. Loening AM, Gambhir SS (2003) AMIDE: A free software tool for multimodality medical image analysis. *Mol Imaging* 2:131–137.
42. Maes F, Collignon A, Vandermeulen D, Marchal G, Suetens P (1997) Multimodality image registration by maximization of mutual information. *IEEE Trans Med Imaging* 16:187–198.